I&EC research
Industrial & Engineering Chemistry Research

Article

Cite This: Ind. Eng. Chem. Res. 2018, 57, 8190−8199

pubs.acs.org/IECR

In Situ Aluminum Migration into Zeolite Framework during Methanol-To-Propylene Reaction: An Innovation To Design Superior Catalysts

Junjie Li,[†] Min Liu,*[,†] Xinwen Guo,[†] Chengyi Dai,[†] Shutao Xu,[‡] Yingxu Wei,[‡] Zhongmin Liu,[‡] and Chunshan Song*[,†,§]

[†]State Key Laboratory of Fine Chemicals, PSU-DUT Joint Center for Energy Research, School of Chemical Engineering, Dalian University of Technology, Dalian 116024, People's Republic of China

[‡]State Key Laboratory of Catalysis, Dalian Institute of Chemical Physics, Chinese Academy of Sciences, Dalian 116023, People's Republic of China

[§]Department of Energy and Mineral Engineering, EMS Energy Institute, PSU-DUT Joint Center for Energy Research, Pennsylvania State University, University Park, Pennsylvania 16802, United States

Supporting Information

ABSTRACT: This work involves methanol-to-propylene (MTP) conversion over aluminosilicate MFI (ZSM-5), borosilicate MFI (B-ZSM-5), and all-silica MFI (Silicate-1). Both B-ZSM-5 and Silicate-1 were inactive in MTP reaction. However, extruded Silicate-1 sample prepared by extrusion with Al_2O_3 binder, followed by acid washing treatment, displayed a rapid increase in methanol conversion in the initial 30 h time on stream (TOS), and then retained 99% methanol conversion, higher propylene selectivity (52.2%), and higher propylene/ethylene ratio (11.3) for 400 h TOS. Silicate-1 modified with $AlCl_3$ or $Al(NO_3)_3$ showed similar catalytic performance as the extruded samples. Several $AlCl_3$-modified Silicate-1 samples after various TOS values were regenerated and characterized by NH_3-termperature-programmed desorption (TPD), Fourier transform infrared (FT-IR) spectroscopy, and ^{27}Al magic angle spinning nuclear magnetic responance (MAS NMR). The results point to continuous aluminum insertion into Silicate-1 framework during reaction in situ, which rationalizes the superior catalytic performance. By analyzing catalytic performances of $AlCl_3$-modified samples with different amounts of defect sites, we concluded that Al migration is related to the defect sites. Finally, a catalyst with a much longer lifetime of 960 h and 53.2% propylene selectivity was developed by incorporating Al migration into hierarchical samples.

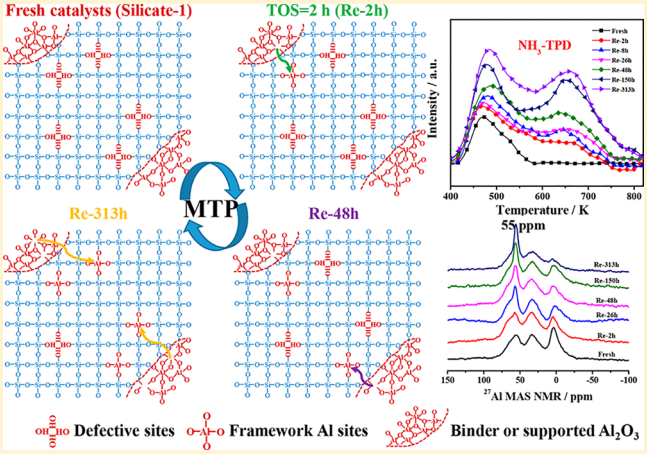

1. INTRODUCTION

Zeolites have been widely used in the refinery and petrochemical industries, which benefit from their special pore structure and intrinsic acidity. From syngas to methanol and methanol to hydrocarbon processes (MTH), higher selectivity of gasoline-range hydrocarbons (methanol-to-gasoline, MTG),[1] light olefins (methanol-to-olefins, MTO) or aromatics (methanol-to-aromatics, MTA) can be achieved,[2−5] which relieves the petroleum crisis because of abundant feedstock (coal, natural gas, and biomass). MTO and MTP technologies have attracted significant attention, because of the increasing demand for ethylene and propylene. SAPO-34 and ZSM-5 serve as two successful catalysts. However, it is still a challenge for further enhancement of stability and propylene selectivity for MTP catalysts.[6−8]

For zeolite catalysts, porosity and acidity determine the catalytic stability and product distribution.[4,9] Purely microporous structure suffer from ineffective diffusion, especially for carbon precursors that lead to fast deactivation.[10−12] Recently, numerous efforts have been reported to improve diffusion property by synthesizing nanocrystals or nanosheets,[13−15] and by introducing mesopores into the microporous structure.[16−20] Templating methods (hard templating, supramolecular templating, and indirect templating) and post-synthesis methods (acid or base leaching) have been reported for obtaining hierarchical structures. Among the approaches mentioned above, mesopore formation by simple base leaching has attracted much attention. After original work by Matsukata and co-workers in 2000,[21] numerous studies have been

Received: January 31, 2018
Revised: May 26, 2018
Accepted: May 31, 2018
Published: May 31, 2018

DOI: 10.1021/acs.iecr.8b00513
Ind. Eng. Chem. Res. 2018, 57, 8190−8199

performed to introduce mesopore structure via desilication. An optimal Si/Al ratio of 25−50 is the most important factor for desilication.[22] Restricted silica removal and minor mesopores were introduced into ZSM-5 with lower Si/Al ratio that was attributed to excessive protection of Al, while the occurrence of uncontrollable dissolution leads to high-silica ZSM-5 with larger pores and lower solid yield.[23−25] Hierarchical zeolites have been widely examined in heterogeneous catalysis reactions, and substantial enhancement of catalytic stability can be achieved because of a higher coke tolerance and an increased diffusion rate of coke precursors.[26−29]

Acid properties, including acid density, acid strength, acid distribution, and acid accessibility, represent an important factor that affects catalytic activity, stability, and selectivity.[30−32] Catalytic activity increases as the number of acid sites increases.[3,33] However, higher acid density facilitates condensation reactions of coke precursors that can result in fast deactivation.[33] As was reported, there are two mechanistic cycles—aromatic-based reaction and alkene-based reaction—running simultaneously during the MTH reaction.[34,35] Ethylene mainly came from the aromatic-based reaction, while the alkene-based reaction involved only C3+ olefins (light olefins without ethylene). Catalysts with higher acid density lead to more reactions of methylbenzenes over active sites before diffusing out of the micropores; in other words, it enhances the proportion of aromatic-based reactions that result in higher ethylene selectivity but lower propylene selectivity.[36] Catalysts with higher acid strength led to quick deactivation and lower olefins selectivity, because of many more hydrogen transfer reactions. Several groups found that higher acid strength facilitates aromatic-based reactions, which lead to higher ethylene selectivity but lower propylene selectivity.[6,37−39] The significant influence on catalytic performance over different acid sites that are located at channels or intersections has been studied recently.[40,41] A larger amount of coke precursors was generated at intersections, which resulted in quick deactivation.[40] Besides, ZSM-5 with larger amounts of acid sites located at intersections facilitated aromatics-based reactions that resulted in lower propylene/ethylene ratios.[41] Al pairs and single Al also affected acid-type or redox-type catalytic reactions.[42,43]

Numerous work has been reported on flexible tuning acidity by in situ synthesis, metal modification, steaming treatment, or acid washing. By contrast, there has been relatively fewer studies on acidity modification by controlling Al insertion into silica-rich zeolite for the improvement of catalytic performance. Several articles reported Al insertion into high-silica ZSM-5 or B-ZSM-5 framework through gas−solid reaction with aluminum halide vapor or gas−liquid reaction with aqueous fluoaluminates, which showed similar catalytic performance, compared with as-synthesized ZSM-5 with similar acidity.[44−46] However, to the best of our knowledge, few studies have focused on in situ Al insertion into zeolite structure during high-temperature reaction. ZSM-5 with lower Si/Al showed a long period of propylene selectivity growth stage before reaching steady state, finally resulting in lower average propylene selectivity. In addition, it showed faster coke deposition rate. While steady higher propylene selectivity and slower coke deposition rate were achieved for ZSM-5 with higher Si/Al (≥300), but it showed a shorter lifetime, because of limited acid sites. If some new active sites were introduced into those high-silica catalysts once methanol conversion decreased, a catalyst with longer lifetime and steady higher propylene selectivity would be obtained. Following this idea, we designed superior catalysts with much longer lifetime, constant higher propylene selectivity, and higher propylene/ethylene ratio by controlling aluminum migration from the binder or supported aluminum into a MFI framework during MTP reaction, and Al migration occurred during the reaction, which meant continuous aluminum insertion with time on stream (TOS).

In this study, TPAOH templated Silicate-1 was extruded with pseudo-boehmite, acid-washed, and evaluated in MTP reaction. $AlCl_3$ or $Al(NO_3)_3$ modified Silicate-1 was also evaluated in MTP reaction. In order to demonstrate continuous Al migration during MTP reaction, several $AlCl_3$-modified Silicate-1 samples via various TOS values were regenerated and characterized by NH_3-TPD, ^{27}Al MAS NMR, and OH-IR. Besides, fluoride-mediated F-Silicate-1, B-ZSM-5, acid-treated B-ZSM-5, NH_4F-modified Silicate-1-NH_4F, and high-temperature (1073 K) calcined Silicate-1−1073K with different amounts of defect sites were modified with $AlCl_3$ and evaluated in MTP reaction, which was used to study the relationship between Al migration and defect sites. For further enhancement of catalytic performance, continuous Al migration was introduced into hierarchical catalysts.

2. EXPERIMENTAL SECTION

2.1. Catalyst Preparation. All-silica MFI (Silicate-1) was synthesized as follows. 38.23 g tetrapropylammonium hydroxide (TPAOH) solution (25% in H_2O), 3.02 g of H_2O, and 36.00 g of tetraethoxysilane (TEOS) were mixed and hydrolyzed at 308 K for 3 h, then 82.50 g of H_2O was poured into the mixture. After stirring at 308 K for 90 min, the mixture was heated to 363 K for alcohol removal; finally, water was added to the original volume and the mixture was transferred into a 200 mL Teflon-lined steel autoclave. After crystallization at 443 K for 72 h, the powder was obtained by centrifugation, drying at 373 K overnight, and calcination at 813 K for 4 h. Silicate-1−1073K was received via an additional calcination step at 1073 K for 120 min. NH_4F treatment was operated by mixing 10 g of Silicate-1 with 200 mL of 0.06 mol/L NH_4F solution, stirring at room temperature for 10 h, drying at 373 K overnight, and calcining at 873 K for 6 h; the modified sample was labeled as Silicate-1−NH_4F.

Fluoride-mediated Silicate-1 was synthesized as follows. First, 16.03 g TEOS was put into a 250 mL conical flask to mix with 1.44 g of tetrapropylammonium bromide (TPABr) and 5.74 g of TPAOH (25 wt % in water), then 1.92 g of nanosized Silicate-1 suspension (with narrow particle size distribution at 70 nm) and 45.0 g of H_2O were added dropwise into the flask under magnetic stirring. After hydrolysis at room temperature for 3 h, a solution containing 3.19 g of NH_4F and 60.93 g of H_2O was added dropwise into the silica gel, followed by 90 min of stirring. The obtained gel was transferred to a 200 mL Teflon-lined autoclave and kept at 443 K for 48 h. The powder was obtained via centrifugation and drying at 373 K overnight. TPA^+ was removed by calcination at 813 K for 6 h. The sample was labeled as F-Silicate-1.

B-ZSM-5 was synthesized as follows. 13.34 g of TPABr was added into 66.67 g of colloidal silica solution (30% in H_2O) and hydrolyzed at 308 K for 30 min. A solution containing 34.25 g of ethylamine aqueous (65% in H_2O), 1.65 g of boric acid, and 45.00 g of H_2O then was added dropwise into the silica gel. Finally, 1 wt % amounts of the nano Silicate-1 suspension were poured into the mixture and stirred for 90

DOI: 10.1021/acs.iecr.8b00513
Ind. Eng. Chem. Res. 2018, 57, 8190−8199

min. The received gel was transferred into a Teflon-lined stainless-steel autoclave and crystallized at 443 K for 72 h. The powder was received by the same procedure mentioned above. Acid washing by 0.2 mol/L HCl or 2.0 mol/L HCl was performed at 348 K for 8 h with a liquid-to-solid ratio of 30 mL/g, and the samples were labeled as B-ZSM-5−0.2HCl and B-ZSM-5−2.0HCl. A B-ZSM-5-AT1 sample was obtained by 0.2 mol/L NaOH treatment of parent B-ZSM-5 at 338 K for 30 min with a liquid-to-solid ratio of 30, while a B-ZSM-5-AT2 sample was obtained by 0.15 mol/L NaOH treatment with additional 0.05 mol/L TPAOH. All of the samples were exchanged to H-type before characterization and evaluation, which was obtained by three repeated ion exchange with 1.0 mol/L NH_4NO_3 solution at 353 K for 1.5 h, followed by drying overnight and calcination at 813 K for 4 h.

Extrusion was performed in a homemade apparatus. Typically, the powder and binder pseudoboehmite with a dry mass ratio of 5:2 were homogenized and mixed with 10% HNO_3 aqueous solution. After that, shaping catalysts were calcined at 813 K for 4 h after natural drying for 48 h and 373 K drying for 12 h. Mild acid washing then was performed by 2.0 mol/L HCl or HNO_3 washing at 353 K with a liquid-to-solid ratio of 10. The extruded sample was labeled as A-Ex, and acid-treated A-Ex was labeled as A-Ex-HCl or A-Ex-HNO_3. ^{27}Al MAS NMR spectroscopy is the most effective characterization method to prove Al incorporation into the zeolite framework; however, background interference on characteristic spectra from larger amounts of Al in the binder brought great obstacles, because it was difficult to separate limited framework four-coordinate Al sites from large amounts of extra-framework Al in the Al_2O_3 binder. $AlCl_3$- or $Al(NO_3)_3$ (1.5 wt % Al)-modified samples were prepared for a detailed study. $AlCl_3$/Silicate-1, $Al(NO_3)_3$/Silicate-1, $AlCl_3$/Silicate-1-NH_4F, $AlCl_3$/Silicate-1−1073K, $AlCl_3$/F-Silicate-1, $AlCl_3$/B-ZSM-5, $AlCl_3$/B-ZSM-5−0.2HCl, and $AlCl_3$/B-ZSM-5−2.0HCl were received by incipient impregnation of the samples with $AlCl_3{\cdot}6H_2O$ or $Al(NO_3)_3{\cdot}9H_2O$ solution (containing 1.5 wt % Al) and drying overnight at 373 K. Samples without reaction were labeled as "Fresh", and regenerated (calcined at 873 K for 6 h) samples after various reaction time (#h) were labeled as Re-#h (where the prefix "Re" denotes regenerated and the suffix "#h" denotes the reaction time (in hours).

2.2. Catalyst Characterization. All of the catalysts were measured by X-ray diffraction (XRD) using a RIGAKU D/Max 2400 diffractometer, equipped with a Cu Kα X-radiation (1.542 Å) source operating at 40 kV and 100 mA. The powder diffractograms were recorded from 5° to 50°. Scanning electron microscopy (SEM) images were obtained on a Hitachi S-5500 instrument with an acceleration voltage of 3 kV or a cold field-emission Hitachi SU8200 instrument with an acceleration voltage of 5 kV. Transmission electron microscopy (TEM) images were taken on a Tecnai G2 20 S-twin instrument (FEI Company) with an acceleration voltage of 200 kV. Images with higher magnification were taken on JEM-2100F instrument (JEOL Company) with an acceleration voltage of 200 kV. The samples for TEM analysis were prepared by dripping ethanol solutions of the samples onto the carbon-coated copper grids and drying in the air. Ar isotherms were measured with a Quantachrome Autosorb Q2 gas adsorption analyzer at 87 K. Prior to the measurement, the samples were degassed under vacuum at 573 K for 8 h. The elemental analysis of alkaline solutions was conducted on a PerkinElmer OPTIMA 2000DV ICP optical emission spectrometer. The chemical compositions of the samples were analyzed by X-ray fluorescence (XRF) spectroscopy on a SRS-3400 X-ray fluorometer. X-ray photoelectron spectroscopy (XPS) measurements were performed on Escalab 250 (Thermo Fisher VG) with a base pressure of 2.4×10^{-8} Pa.

Temperature-programmed desorption of NH_3 was performed on a CHEMBET 3000 chemical absorber (Quantachrome, USA). Approximately 0.1 g of the catalyst sample was pretreated in helium at 773 K for 1 h, cooled to 393 K, then exposed to ammonia−helium mixture (8% NH_3−92% He) for 30 min. The physically adsorbed NH_3 was removed by helium flow at 393 K for 1 h. The TPD plot was obtained with a heating rate of 10 K/min from 393 K to 923 K. The desorbed ammonia was detected by gas chromatography with a thermal conductivity detector. The OH-IR spectra were recorded with an EQUINOX55 (Bruker) Fourier transform infrared spectrometer by means of the KBr pellet technique. Prior to the measurements, the samples were heating to 573 K under vacuum ($\sim 1.33 \times 10^{-3}$ Pa) for 1 h. The spectra of all samples were presented by subtracting the background spectrum.

^{27}Al MAS NMR measurements were performed on a 600 MHz Bruker Avance III equipped with a 4 mm MAS probe at a spinning rate of 12 kHz, using a one-pulse sequence. 200 scans were accumulated with a $\pi/8$ pulse width of 0.75 μs and a recycle delay of 2 s.[47−50] The chemical shifts were referenced to $(NH_4)Al(SO_4)_2{\cdot}12H_2O$ at −0.4 ppm.[51]

2.3. Catalytic Tests. Methanol conversion to propylene reaction was performed on a fixed-bed continuous-flow reactor with a stainless steel tube. In a typical run, 1 g of each catalyst (size 10−20 mesh) was loaded in the flat-temperature zone of the reactor. Prior to the test, the catalyst was activated in situ with a heating rate of 4 K/min to 773 K, and kept for an hour, then methanol−water mixture (molar ratio 1:1) was injected into the reactor by a Lab Alliance Series II pump to provide methanol weight hourly space velocity (WHSV) of 3.0 h^{-1}. The tests were conducted at 773 K under atmospheric pressure, the gas products were analyzed by a gas chromatograph (GC) equipped with a flame ionization detector (FID) and a HP-PLOT Q capillary column 30 m in length. The liquid products were analyzed by a GC equipped with a FID and a 2 m HayeSep Q packing column. Both methanol and dimethyl ether (DME) were regarded as reactants for conversion calculation.

3. RESULTS AND DISCUSSION

3.1. Characterization and Catalytic Performance of Extruded Samples. Figure S1 in the Supporting Information shows the XRD patterns of Silicate-1, F-Silicate-1, and B-ZSM-5. All of the samples exhibited typical MFI topology. Ar adsorption−desorption isotherms of the three samples are shown in Figure S2 in the Supporting Information. All of the samples displayed type I adsorption isotherms, which is typical for microporous materials. The difference in defective sites for the three samples was detected from FT-IR results, in the region of 3800−3000 cm^{-1} corresponding to OH vibration; there were four main bands for aluminosilicate ZSM-5 (see Figure 1). The first broad band at ~3535 cm^{-1} belonged to silanol nests that were composited by several silanol groups through extended hydrogen bonding.[52] The second band at 3600 cm^{-1} was attributed to framework aluminum hydroxyl that is related with Brönsted acid sites. The last broad band at 3700−3740 cm^{-1} consisted two bands at 3725 and 3734 cm^{-1}, which were attributed to internal silanol groups and terminal silanol groups, respectively. Notably, there was no bands at

DOI: 10.1021/acs.iecr.8b00513
Ind. Eng. Chem. Res. 2018, 57, 8190−8199

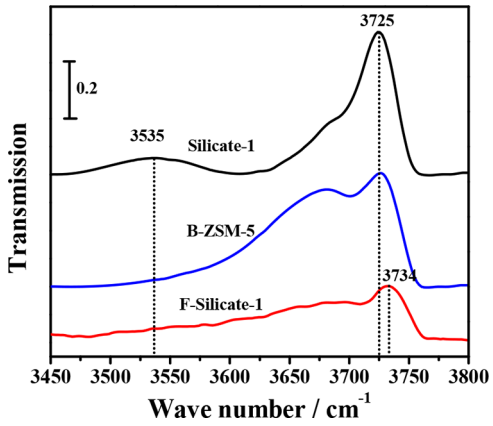

Figure 1. Fourier transform infrared (FT-IR) spectra in the OH region for different samples.

3600 cm^{-1} for F-Silicate-1, Silicate-1, or B-ZSM-5, which illustrated few framework aluminum hydroxyls. Silicate-1 had an obvious band at 3535 cm^{-1}, which represented larger amounts of silanol nests, compared with F-Silicate-1 and B-ZSM-5. F-Silicate-1 showed only one obvious band at 3734 cm^{-1}; it demonstrated that F-Silicate-1 had few silanol nests and internal silanol groups.[13,53] Table S1 in the Supporting Information shows physicochemical properties of the three samples. There was no Al detected for Silicate-1 and F-Silicate-1, while B-ZSM-5 had a high Si/Al ratio (1158), which was caused by Al impurities in silica sol. Silicate-1 showed a slightly higher BET surface area and micropore volume, compared with F-Silicate-1 and B-ZSM-5. SEM images of those samples are shown in Figure S3 in the Supporting Information. Silicate-1 displayed spherical-shaped crystals with a uniform particle size of ~160−180 nm, F-Silicate-1 showed regular coffin-shape crystals with sizes of 80 nm × 200 nm × 400 nm, and B-ZSM-5 showed nanoaggregates with a particle size of ~450 nm.

Powder Silicate-1 and F-Silicate-1 without framework Al sites were inactive in MTP reaction. Figure 2 shows the catalytic performance of the extruded samples. As shown in Figure 2a, F-Silicate-1-Ex showed lower methanol conversion in the initial stage, and the methanol conversion quickly decreased to zero. Additional HCl washing of F-Silicate-1-Ex-HCl hardly improved methanol conversion. Silicate-1-Ex showed similar low activity in MTP reaction. However, it was interesting that Silicate-1-Ex-HCl exhibited a much higher initial methanol conversion (41%), and it increased to >90% after 20 h TOS, then 99% methanol conversion was maintained for ~400 h TOS. Besides, it also exhibited higher propylene selectivity (52.2%), lower methane selectivity (0.4%), and lower ethylene selectivity (4.6%) at the stable stage (Figure 2b). In addition, it showed a higher P/E ratio of 11.3, compared to previous results.[3,8,54−57] HNO_3-treated Silicate-1-Ex-HNO_3 also displayed similar catalytic performance as Silicate-1-Ex-HCl. Thus, it could be concluded that extrusion with Al_2O_3 binder and sequential acid washing brought superior catalytic performance to inactive Silicate-1 during MTP reaction. Why did Silicate-1-Ex-HCl and Silicate-1-Ex-HNO_3 show outstanding catalytic performance? Did it correlate with Al migration from Al_2O_3 binder into Silicate-1 framework? If it was attributed to Al migration, it occurred over what kind of catalysts? In order to determine the relationship between Al migration and superior catalytic performance of extruded Silicate-1, $AlCl_3$- or $Al(NO_3)_3$-modified samples were prepared and evaluated in MTP reaction for reducing background interference on characteristic spectra from larger amounts of Al in the binder.

3.2. Characterization and Catalytic Performance of Al-Supported Samples. Methanol conversion with TOS for $AlCl_3$-modified samples are shown in Figure 3. A lower initial methanol conversion was observed for $AlCl_3$/F-Silicate-1, and it decreased to zero after 20 h TOS, which was similar to F-

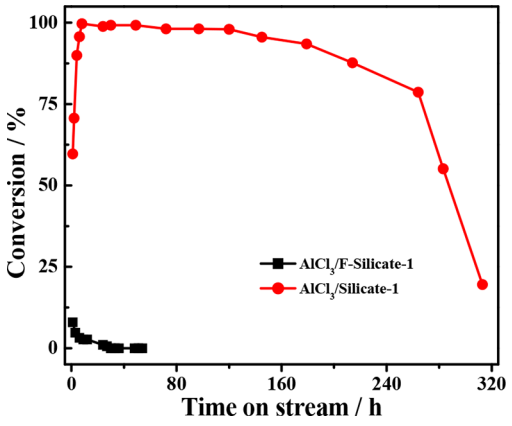

Figure 3. Methanol conversion versus time on stream (TOS) over $AlCl_3$-modified samples.

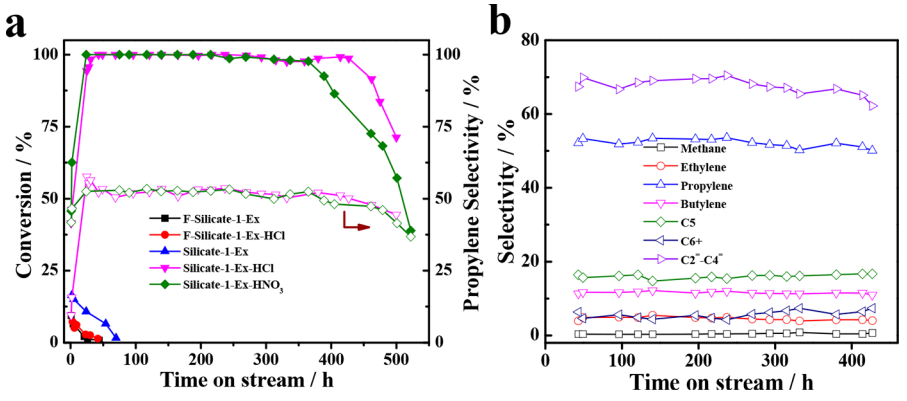

Figure 2. Catalytic performance of extruded samples with or without acid washing: (a) methanol conversion and (b) propylene selectivity and product selectivity over Silicate-1-Ex-HCl versus time on stream (TOS). The solid symbols represent methanol conversion, and the open symbols represent propylene selectivity.

DOI: 10.1021/acs.iecr.8b00513
Ind. Eng. Chem. Res. 2018, 57, 8190−8199

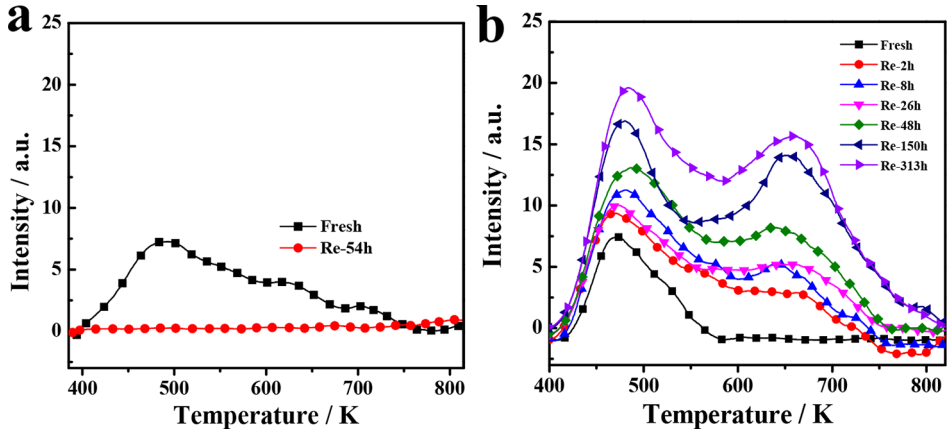

Figure 4. NH_3-TPD profiles of fresh samples and regenerated samples after various reaction time: (a) $AlCl_3$/F-Silicate-1 and (b) $AlCl_3$/Silicate-1.

Silicate-1-Ex and F-Silicate-1-Ex-HCl. While $AlCl_3$/Silicate-1 gave higher initial conversion of 60.0% and quickly increased to 100% within 8 h TOS. The decrease of methanol conversion appeared after 180 h TOS. As shown in Figure S4 in the Supporting Information, $Al(NO_3)_3$/Silicate-1 gave lower methanol conversion of 23% in the initial stage, but nearly 100% methanol conversion was reached after 10 h TOS; significant decrease of conversion happened after 80 h TOS which was shorter than that with $AlCl_3$/Silicate-1.

NH_3-TPD analysis was used to determine the reasons of the enhancement of catalytic performance after $AlCl_3$ modification. Figure 4a shows acid properties of fresh $AlCl_3$/F-Silicate-1 and regenerated $AlCl_3$/F-Silicate-1-Re. Both of the samples possessed less strong acidity, which explained lower activity of $AlCl_3$/F-Silicate-1. Figure 4b shows acid properties of regenerated $AlCl_3$/Silicate-1 samples after various TOS, and Table 1 lists the amount of acid based on NH_3-TPD results.

Table 1. Acid Amounts of Fresh and Regenerated $AlCl_3$/Silicate-1 Based on NH_3-TPD Results

catalyst	total acidity (μmol/g)	weak acidity (μmol/g)	strong acidity (μmol/g)
Fresh	9.9	9.9	0
Re-2h	24.9	15.8	9.1
Re-8h	26.0	14.2	11.8
Re-26h	28.3	16.2	12.1
Re-48h	34.0	18.6	15.4
Re-150h	46.3	21.7	24.6
Re-313h	54.7	25.4	29.3

Fresh $AlCl_3$/Silicate-1 showed only one NH_3 desorption peak at 480 K that belonged to weak acid sites, and the amount of acid was 9.9 μmol/g, as displayed in Table 1. For regenerated $AlCl_3$/Silicate-1 after 2 h TOS (Re-2h), another peak at higher temperature that belonged to strong acidity appeared, and Table 1 showed 15.8 μmol/g weak acid sites and 9.1 μmol/g strong acid sites. While Re-8h showed a larger peak at higher temperature, which pointed to more strong acid sites of Re-8h, compared with Re-2h. The amounts of weak and strong acid sites increased with prolonged TOS. Maximum NH_3-TPD desorption peaks at both lower and higher temperature were obtained for Re-313h. It possessed 29.3 μmol/g strong acid sites and 25.4 μmol/g weak acid sites (Table 1), which corresponded to conventional ZSM-5 with Si/Al ratio of 200. It can be speculated that enhanced activity was attributed to increased strong acid sites, which may be achieved by Al migration from $AlCl_3$ or $Al(NO_3)_3$ into zeolite framework. ^{27}Al MAS NMR was used to directly demonstrate gradual Al insertion into framework structure during reaction.

Figure 5 shows ^{27}Al MAS NMR spectra of fresh $AlCl_3$/Silicate-1 and regenerated samples after various TOS. The

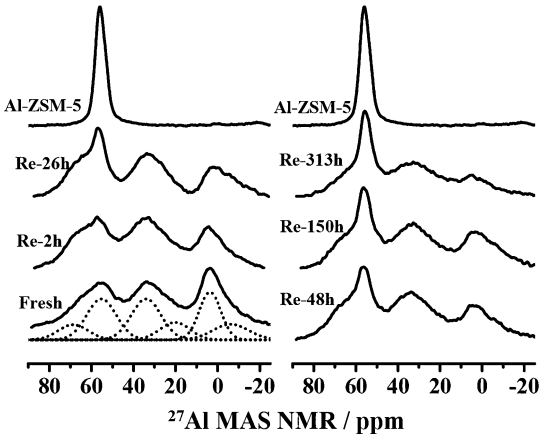

Figure 5. ^{27}Al MAS NMR spectra of fresh and regenerated $AlCl_3$/Silicate-1 samples after various reaction TOS values. The ^{27}Al MAS NMR spectrum of Al-ZSM-5 is taken from our previous work.[54]

spectrum of reference Al-ZSM-5 showed a single and narrow peak at 55 ppm that was attributed to four-coordinate Al site in the framework, which was coordinated by four −O−Si− species.[54] The spectrum of fresh $AlCl_3$/Silicate-1 showed several broad peaks that were attributed to four-coordinate Al(IV), five-coordinate Al(V), and six-coordinate Al(VI) environments, respectively.[58−60] Those different aluminum species were coordinated by −O−Al− or −Cl, and a part of Al at the interface of Silicate-1 was coordinated to −O−Al−, −Cl, or −O−Si− species.[61,62] A small sharp peak at 55 ppm appeared for Re2h, compared with fresh $AlCl_3$/Silicate-1, and the intensity of this peak became stronger for Re-26h and is the largest for Re-313h. Based on the spectrum of Al-ZSM-5 reference, it can be concluded that larger amounts of framework four-coordinate Al sites were generated after longer TOS, which pointed to continuous insertion of Al into zeolite framework structure during MTP reaction in situ.

Al insertion into zeolite framework was also demonstrated by FT-IR studies. As shown in Figure S5 in the Supporting

DOI: 10.1021/acs.iecr.8b00513
Ind. Eng. Chem. Res. 2018, 57, 8190−8199

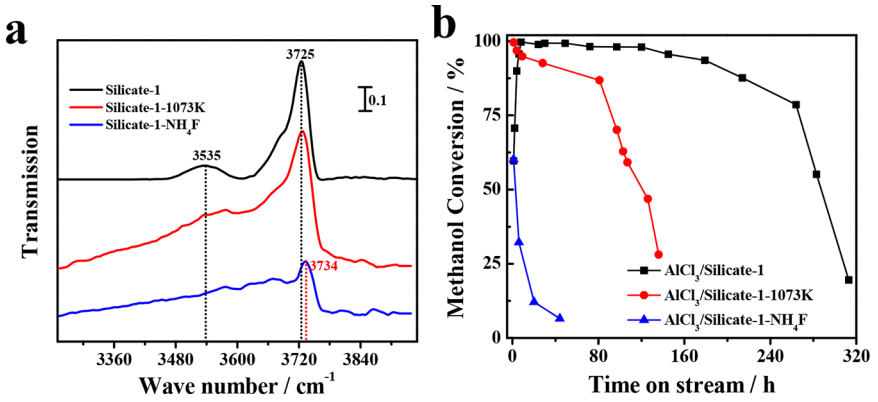

Figure 6. (a) OH-IR spectra of Silicate-1 via different treatment methods, and (b) catalytic performance of $AlCl_3$-impregnated samples.

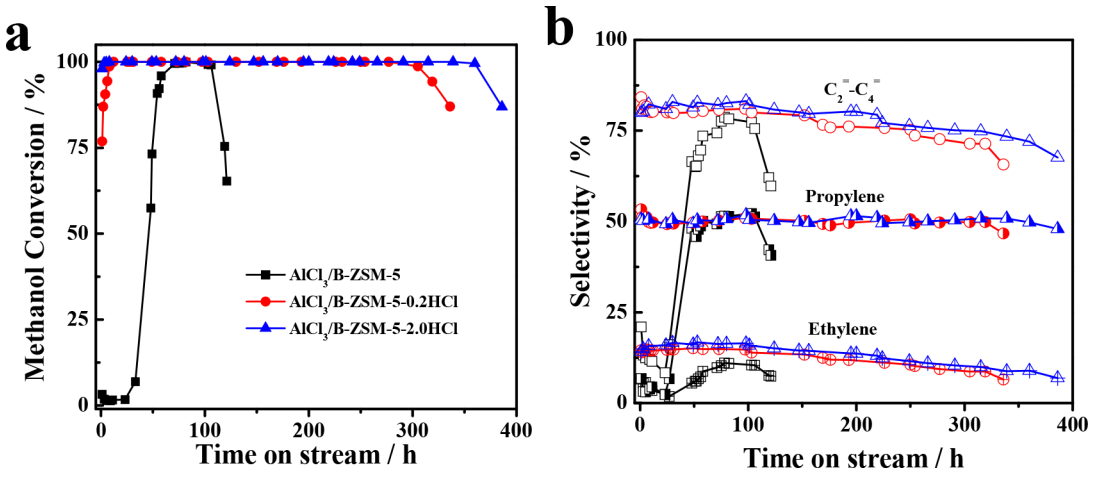

Figure 7. Catalytic performance of $AlCl_3$-impregnated parent B-ZSM-5 and acid-treated B-ZSM-5: (a) methanol conversion versus TOS for different samples, and (b) product selectivity versus TOS for those samples.

Information, the band at 3535 cm^{-1} changed slightly after $AlCl_3$ modification. For the Re-313 sample, the band at 3535 cm^{-1} that belonged to silanol nests disappeared. Moreover, the band at 3730 cm^{-1} attributed to silanol groups was significantly reduced after reaction. However, a small band at 3600 cm^{-1} appeared, which proved Al insertion into framework structure. Thus, it can be concluded that, over the special catalytic performances of $AlCl_3$/Silicate-1 and $Al(NO_3)_3$/Silicate-1, samples were attributed to gradual Al insertion into the zeolite framework during reaction.

Figure S6 in the Supporting Information shows the catalytic performances of conventional ZSM-5 with different Si/Al. ZSM-5 with lower Si/Al showed lower propylene selectivity at the initial reaction time, and there was a long period of propylene selectivity growth stage. Steady higher propylene selectivity was obtained for ZSM-5 with higher Si/Al (≥300); however, it exhibited a shortened lifetime that was attributed to limited acid sites of those samples. If some new active sites were generated once the methanol conversion reduced for ZSM-5 with higher Si/Al (⩾300), a catalyst with steady higher propylene selectivity and longer lifetime would be obtained. Therefore, higher propylene selectivity and longer lifetime of extruded or $AlCl_3$-modified Silicate-1 were attributed to gradual Al insertion into the zeolite framework, which served as new active sites.

3.3. Relationship between Al Insertion and Defect Sites. Al migration occurs over what type of zeolites? By analysis of the different catalytic performance of extruded F-Silicate-1 and Silicate-1, it can be speculated that Al migration may maintain a close relationship with defect sites. In order to prove this viewpoint, $AlCl_3$-impregnated Silicate-1-NH_4F and Silicate-1−1073K with different amounts of defect sites were evaluated in MTP reaction. Figure 6a shows FT-IR results of those samples. For Silicate-1−1073K, the intensity of the band at 3535 cm^{-1} decreased after high-temperature calcination, which was attributed to silicon hydroxyl condensation reactions.[63] While the band at 3535 cm^{-1} disappeared for fluorinated Silicate-1-NH_4F, it also showed a small band at ~3734 cm^{-1} without a shoulder peak at 3725 cm^{-1}, indicative of selective removal of internal hydroxyl groups of NH_4F modification.[54] The catalytic performances of the three catalysts are shown in Figure 6b. $AlCl_3$/Silicate-1−1073K exhibited higher methanol conversion in the initial stage, compared with $AlCl_3$/Silicate-1, but it decreased below 20% after 140 h TOS. While similar initial methanol conversion was obtained for $AlCl_3$/Silicate-1-NH_4F, compared with $AlCl_3$/Silicate-1, the methanol conversion quickly decreased to 6.5% within 48 h TOS.

For further research, acid-treated samples B-ZSM-5−0.2HCl and B-ZSM-5−2.0HCl with more defect sites were modified with $AlCl_3$ and evaluated in MTP reaction. Figure 7 shows catalytic performance of sample $AlCl_3$/B-ZSM-5, $AlCl_3$/B-ZSM-5−0.2HCl, and $AlCl_3$/B-ZSM-5−2.0HCl. As shown in Figure 7a, $AlCl_3$/B-ZSM-5 displayed steady low methanol

DOI: 10.1021/acs.iecr.8b00513
Ind. Eng. Chem. Res. 2018, 57, 8190−8199

conversion in the initial 24 h TOS, and then distinct growth appeared after 48 h TOS. 100% methanol conversion was obtained after 70 h TOS and maintained for 40 h. By contrast, an initial higher methanol conversion of 77% was obtained for $AlCl_3$/B-ZSM-5−0.2HCl, the methanol conversion reached 100% after 10 h TOS and was maintained for 300 h. $AlCl_3$/B-ZSM-5−2.0HCl exhibited almost 100% methanol conversion after 1 h TOS, and 100% methanol conversion was maintained for ∼380 h. Figure 7b shows products distribution results of the three catalysts. Both of $AlCl_3$/B-ZSM-5−0.2HCl and $AlCl_3$/B-ZSM-5−2.0HCl showed higher propylene selectivity of 50.5% and $C2^{=}$-$C4^{=}$ (ethylene, propylene, and butylene) selectivity of 78.1%, compared with conventional high-silica ZSM-5.

FT-IR spectra of parent and modified B-ZSM-5 are shown in Figure 8. B-ZSM-5 had few silanol nests, but a broad band at

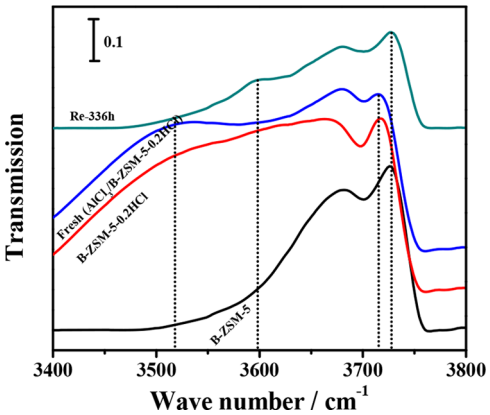

Figure 8. FT-IR in the OH region for different samples.

∼3530 cm^{-1} belonged to silanol nests that appeared after HCl washing, which was attributed to boron removal. The band at ∼3530 cm^{-1} slightly changed after $AlCl_3$ modification, and there was no band at ∼3600 cm^{-1} that belonged to framework aluminum hydroxyl. While the band at 3535 cm^{-1} disappeared after long-time TOS for regenerated $AlCl_3$/B-ZSM-5−0.2HCl after 336 h TOS (Re-336h), besides an obvious band at 3600 cm^{-1} that appeared, it pointed to Al insertion into the framework structure during reaction. Therefore, it can be concluded that Al insertion maintained a close relationship with defect sites. The acid properties of parent B-ZSM-5, fresh $AlCl_3$/B-ZSM-5, and regenerated Re-121h are shown in Figure S7a in the Supporting Information. The amounts of weak acid sites were greatly reduced, which was attributed to the removal of some framework B sites in high-temperature water vapor, and generated some silanol nests. And a small NH_3-TPD desorption peak at higher temperature appeared for Re-121h, which explained the special catalytic performance of $AlCl_3$/B-ZSM-5 (Figure 7a). Figure S7b in the Supporting Information shows NH_3-TPD results of B-ZSM-5−0.2HCl, fresh samples ($AlCl_3$/B-ZSM-5−0.2HCl), and regenerated samples (Re-336h). A large amount of strong acid sites appeared after reaction, which explained superior catalytic performance of $AlCl_3$/B-ZSM-5−0.2HCl.

3.4. Al Insertion into Hierarchical Shaping Catalysts. A superior catalyst was obtained by introducing gradual Al migration into hierarchical catalysts. XRD patterns of the samples are shown in Figure S8 in the Supporting Information. All three samples exhibited typical MFI topology; however, the crystallinity varied greatly. AT2 sample showed much lower crystallinity that may be attributed to the existence of more mesopores. SEM and TEM images are shown in Figure 9.

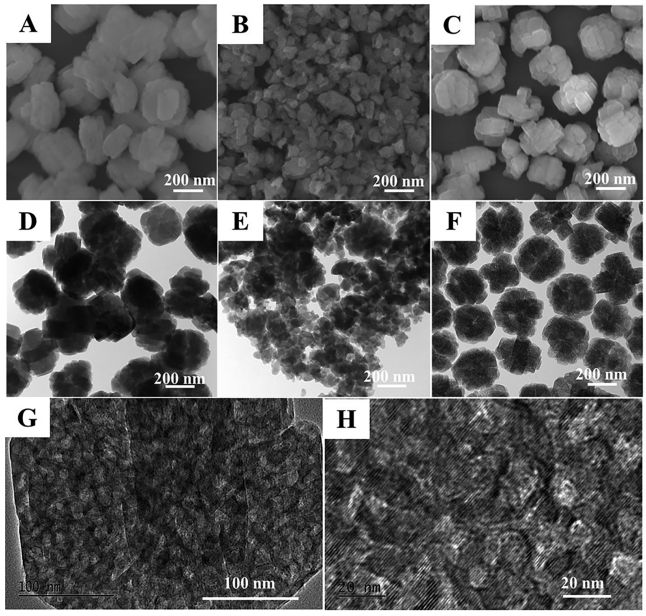

Figure 9. SEM and TEM images of parent and alkaline treated B-ZSM-5 samples: (A, D) parent B-ZSM-5; (B, E) AT1 sample via single NaOH treatment; (C, F) AT2 sample via NaOH + TPAOH treatment; and (G, H) higher-magnification TEM results of the AT2 sample.

Parent B-ZSM-5 in Figure 9A exhibited 400−450 nm spherical aggregates, and TEM results in Figure 9D also illustrated aggregate particles. AT1 sample, via sole NaOH treatment, showed nanofragments in Figure 9B, and the TEM result in Figure 9E proved that OH^- depolymerized aggregate B-ZSM-5 into nanofragments instead of constructing a hierarchical structure. By contrast, the AT2 sample in Figure 9C showed similar morphology as the parent B-ZSM-5, but mesoporous structure was introduced into AT2 sample in Figure 9F. Higher-magnification TEM image in Figures 9G and 9H displayed uniform mesoporous structures, which was attributed to the shield effect of TPA^+ by restricting excessive etching of intercrystalline Si−O−Si.

Detailed information about pore structure was obtained by Ar adsorption/desorption. As shown in Figure 10a, parent B-ZSM-5 exhibited a type I isotherm, and the pore distribution curve (Figure 10b) showed less mesoporous structure. The AT1 sample exhibited a type IV isotherm with larger Ar adsorption at higher partial pressure (P/P_0), which belonged to interparticle pores, according to SEM and TEM results. Pore distribution curve of AT1 showed interparticle pores that were larger than 30 nm. The AT2 sample also exhibited a type IV adsorption−desorption isotherm, and significant enhancement of Ar adsorption between P/P_0 = 0.44 and P/P_0 = 0.75 was achieved, pointing to larger amounts of mesopores of the AT2 sample, compared with the AT1 sample. Moreover, the pore distribution curve displayed a uniform mesopore distribution at ∼8 nm. The Ar adsorption results are shown in Table S2 in the Supporting Information. Parent B-ZSM-5 possessed a higher BET surface area (482 m^2/g), higher micropore volume (0.17 cm^3/g), and less mesopore volume (0.09 cm^3/g). The AT1 sample exhibited a lower BET surface area of 413 m^2/g, but much higher total pore volume than parent B-ZSM-5. The

DOI: 10.1021/acs.iecr.8b00513
Ind. Eng. Chem. Res. 2018, 57, 8190−8199

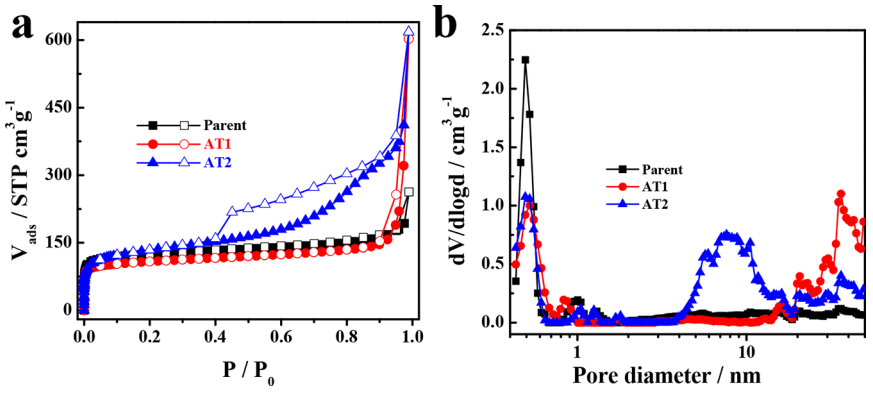

Figure 10. Ar adsorption results of parent and alkaline-treated B-ZSM-5 samples at 87 K. (P_0 = 102.917 kPa): (a) Ar adsorption−desorption isotherms of different samples (the plots with solid symbols represent adsorption isotherms, and the plots with open symbols represent desorption isotherms); (b) pore size distribution results of different samples.

mesoporous surface area was same as parent B-ZSM-5. While the AT2 sample showed a similar BET surface area of 489 cm^2/g as the parent B-ZSM-5, a much higher mesoporous surface area of 150 cm^2/g and mesopore volume of 0.40 cm^3/g were achieved after NaOH + TPAOH treatment.

Parent B-ZSM-5, AT1, and AT2 samples were extruded with pseudoboehmite. All of the catalysts were evaluated in MTP reaction after HCl washing. The catalytic performances of those samples are shown in Figure 11. Inactive powder B-ZSM-5 kept

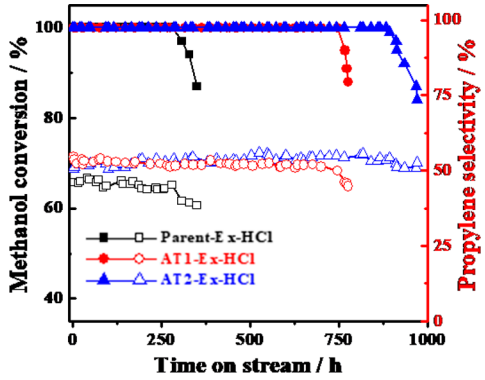

Figure 11. Catalytic performance of shaping parent and alkaline-treated B-ZSM-5. [Plots with solid symbols represent methanol conversion, and the plots with open symbols represent propylene selectivity.]

100% methanol conversion for 300 h after extrusion with pseudoboehmite and acid washing (Parent-Ex-HCl). Table 2 displayed an average propylene selectivity of 44.7%. AT1-Ex-HCl showed much higher stability, with a lifetime of ~775 h, compared with Parent-Ex-HCl, which was attributed to the increased diffusion rate of nanofragments. In addition, it showed much higher propylene selectivity of 51.8% (Table 2).

Table 2. Average Product Selectivity of Different Samples

	Selectivity (%)							
catalyst	CH_4	C_2H_4	C_3H_6	C_4H_8	C2−C4	C5	C6+	P/E
Parent-Ex-HCl	1.2	9.5	44.7	16.8	6.1	15.1	6.6	4.7
AT1-Ex-HCl	0.6	9.0	51.8	15.8	4.5	13.0	5.3	5.8
AT2-Ex-HCl	0.6	7.2	53.2	15.6	5.8	13.5	4.1	7.4

As it is known that two mechanistic cycles ran simultaneously during the MTH reaction over ZSM-5 catalysts, aromatic-based and alkene-based cycles.[34,35] Ethylene mainly came from aromatic-based reactions, and alkene-based reactions generated only C2+ olefins (light olefins without ethylene). Higher diffusion rate reduced the concentration or resident time of methylbenzenes in the pores, which decreased the proportion of aromatic-based reactions but increased the proportion of alkene-based reactions, finally resulted in higher propylene selectivity but lower ethylene selectivity.[64,65] Further improvement of lifetime to 960 h was achieved for the AT2-Ex-HCl sample with mesoporous structure. To the best of our knowledge, it is the most stable catalyst under the reaction conditions of high methanol WHSV of 3 h^{-1} and low H_2O/CH_3OH molar ratio of 1 until now. Moreover, AT2-Ex-HCl possessed highest propylene selectivity of 53.2%, it was attributed to large amounts of mesoporous structure that greatly increased olefin-based reactions. It showed a higher P/E ratio of 7.4 and $C2^=-C4^=$ olefins selectivity of 76.0%.

4. CONCLUSIONS

Gradual Al insertion into the zeolite framework of $AlCl_3$-modified Silicate-1 during methanol-to-propylene reaction was demonstrated by NH_3-TPD, FT-IR, and ^{27}Al MAS NMR characterizations. The various catalytic performance of $AlCl_3$-modified Silicate-1-NH_4F, Silicate-1−1073K, F-Silicate-1, B-ZSM-5, B-ZSM-5−0.2HCl, and B-ZSM-5−2.0HCl was indicative of the close relationship between Al insertion and defect sites. Based on continuous Al migration from the binder into the zeolite framework, extruded Silicate-1 with additional acid washing showed a much longer lifetime of 400 h, a higher propylene selectivity of 52.2%, and a higher P/E ratio of 11.3, compared with conventional high-silica ZSM-5. Further improvement of catalytic performance was achieved by introducing Al migration into hierarchical catalysts. Extruded hierarchical B-ZSM-5 with uniform mesopores showed the longest lifetime (960 h) and the highest propylene selectivity (53.2%). The present work brings a new method for designing and preparing superior catalysts.

■ ASSOCIATED CONTENT

Supporting Information

The Supporting Information is available free of charge on the ACS Publications website at DOI: 10.1021/acs.iecr.8b00513.

DOI: 10.1021/acs.iecr.8b00513
Ind. Eng. Chem. Res. 2018, 57, 8190−8199

XRD, Ar adsorption, and SEM results of Silicate-1, F-Silicate-1, and B-ZSM-5; catalytic performance of $Al(NO_3)_3$/Silicate-1; OH-IR results of $AlCl_3$ modified Silicate-1; catalytic performance of samples with different Si/Al ratio; NH_3-TPD results of B-ZSM-5; XRD and Ar adsorption results of hierarchical B-ZSM-5 (PDF)

AUTHOR INFORMATION

Corresponding Authors

*Fax: +86 0411 84986134. E-mail address: lium@dlut.edu.cn.
*Fax: +1 814 863 4466. E-mail address: csong@psu.edu.

ORCID

Min Liu: 0000-0003-2291-6266
Xinwen Guo: 0000-0002-6597-4979
Chunshan Song: 0000-0003-2344-9911

Author Contributions

The manuscript was written through contributions of all authors. All authors have given approval to the final version of the manuscript.

Notes

The authors declare no competing financial interest.

ACKNOWLEDGMENTS

The authors acknowledge the financial supporting of the National Key Research and Development Program of China (No. 2018YFB060128).

REFERENCES

(1) Topp-Jørgensen, J. Topsøe Integrated Gasoline Synthesis—The Tigas Process. *Stud. Surf. Sci. Catal.* **1988**, *36*, 293–305.
(2) Chang, C. D.; Lang, W. H.; Silvestri, A. J. Synthesis Gas Conversion to Aromatic Hydrocarbons. *J. Catal.* **1979**, *56*, 268–273.
(3) Chang, C. D.; Chu, C. T. W.; Socha, R. F. Methanol Conversion to Olefins over ZSM-5. I. Effect of Temperature and Zeolite SiO_2 Al_2O_3. *J. Catal.* **1984**, *86*, 289–296.
(4) Stocker, M. Methanol-to-Hydrocarbons: Catalytic Materials and Their Behavior. *Microporous Mesoporous Mater.* **1999**, *29*, 3–48.
(5) Tian, P.; Wei, Y.; Ye, M.; Liu, Z. Methanol to Olefins (MTO): From Fundamentals to Commercialization. *ACS Catal.* **2015**, *5*, 1922–1938.
(6) Schulz, H. Coking" of Zeolites During Methanol Conversion: Basic Reactions of the MTO-, MTP- and MTG Processes. *Catal. Today* **2010**, *154*, 183–194.
(7) Wei, Y.; Yuan, C.; Li, J.; Xu, S.; Zhou, Y.; Chen, J.; Wang, Q.; Xu, L.; Qi, Y.; Zhang, Q.; Liu, Z. Coke Formation and Carbon Atom Economy of Methanol-to-Olefins Reaction. *ChemSusChem* **2012**, *5*, 906–12.
(8) Hu, Z.; Zhang, H.; Wang, L.; Zhang, H.; Zhang, Y.; Xu, H.; Shen, W.; Tang, Y. Highly Stable Boron-Modified Hierarchical Nanocrystalline ZSM-5 Zeolite for the Methanol to Propylene Reaction. *Catal. Sci. Technol.* **2014**, *4*, 2891–2895.
(9) Olsbye, U.; Svelle, S.; Bjorgen, M.; Beato, P.; Janssens, T. V.; Joensen, F.; Bordiga, S.; Lillerud, K. P. Conversion of Methanol to Hydrocarbons: How Zeolite Cavity and Pore Size Controls Product Selectivity. *Angew. Chem., Int. Ed.* **2012**, *51*, 5810–31.
(10) Milina, M.; Mitchell, S.; Cooke, D.; Crivelli, P.; Perez-Ramirez, J. Impact of Pore Connectivity on the Design of Long-Lived Zeolite Catalysts. *Angew. Chem., Int. Ed.* **2015**, *54*, 1591–4.
(11) Rownaghi, A. A.; Hedlund, J. Methanol to Gasoline-Range Hydrocarbons: Influence of Nanocrystal Size and Mesoporosity on Catalytic Performance and Product Distribution of ZSM-5. *Ind. Eng. Chem. Res.* **2011**, *50*, 11872–11878.
(12) Milina, M.; Mitchell, S.; Crivelli, P.; Cooke, D.; Pérez-Ramírez, J. Mesopore Quality Determines the Lifetime of Hierarchically Structured Zeolite Catalysts. *Nat. Commun.* **2014**, *5*, 3922.
(13) Qin, Z.; Lakiss, L.; Tosheva, L.; Gilson, J.-P.; Vicente, A.; Fernandez, C.; Valtchev, V. Comparative Study of Nano-ZSM-5 Catalysts Synthesized in OH^- and F^- Media. *Adv. Funct. Mater.* **2014**, *24*, 257–264.
(14) Mintova, S.; Gilson, J.-P.; Valtchev, V. Advances in Nanosized Zeolites. *Nanoscale* **2013**, *5*, 6693–6703.
(15) Choi, M.; Na, K.; Kim, J.; Sakamoto, Y.; Terasaki, O.; Ryoo, R. Stable Single-Unit-Cell Nanosheets of Zeolite MFI as Active and Long-Lived Catalysts. *Nature* **2009**, *461*, 246–249.
(16) Lopez-Orozco, S.; Inayat, A.; Schwab, A.; Selvam, T.; Schwieger, W. Zeolitic Materials with Hierarchical Porous Structures. *Adv. Mater.* **2011**, *23*, 2602–2615.
(17) Moller, K.; Bein, T. Mesoporosity - a New Dimension for Zeolites. *Chem. Soc. Rev.* **2013**, *42*, 3689–3707.
(18) Perez-Ramirez, J.; Christensen, C. H.; Egeblad, K.; Christensen, C. H.; Groen, J. C. Hierarchical Zeolites: Enhanced Utilisation of Microporous Crystals in Catalysis by Advances in Materials Design. *Chem. Soc. Rev.* **2008**, *37*, 2530–2542.
(19) Valtchev, V.; Majano, G.; Mintova, S.; Perez-Ramirez, J. Tailored Crystalline Microporous Materials by Post-Synthesis Modification. *Chem. Soc. Rev.* **2013**, *42*, 263–290.
(20) Wei, Y.; Parmentier, T. E.; de Jong, K. P.; Zecevic, J. Tailoring and Visualizing the Pore Architecture of Hierarchical Zeolites. *Chem. Soc. Rev.* **2015**, *44*, 7234–7261.
(21) Ogura, M.; Shinomiya, S.-y.; Tateno, J.; Nara, Y.; Nomura, M.; Kikuchi, E.; Matsukata, M. Alkali-Treatment Technique — New Method for Modification of Structural and Acid-Catalytic Properties of ZSM-5 Zeolites. *Appl. Catal., A* **2001**, *219*, 33–43.
(22) Groen, J. C.; Peffer, L. A.; Moulijn, J. A.; Perez-Ramirez, J. Mechanism of Hierarchical Porosity Development in MFI Zeolites by Desilication: The Role of Aluminium as a Pore-Directing Agent. *Chem. - Eur. J.* **2005**, *11*, 4983–94.
(23) Pérez-Ramírez, J.; Abelló, S.; Bonilla, A.; Groen, J. C. Tailored Mesoporosity Development in Zeolite Crystals by Partial Detemplation and Desilication. *Adv. Funct. Mater.* **2009**, *19*, 164–172.
(24) Verboekend, D.; Perez-Ramirez, J. Desilication Mechanism Revisited: Highly Mesoporous All-Silica Zeolites Enabled through Pore-Directing Agents. *Chem. - Eur. J.* **2011**, *17*, 1137–1147.
(25) Groen, J. C.; Moulijn, J. A.; Pérez-Ramírez, J. Desilication: On the Controlled Generation of Mesoporosity in MFI Zeolites. *J. Mater. Chem.* **2006**, *16*, 2121.
(26) Cho, H. J.; Dornath, P.; Fan, W. Synthesis of Hierarchical Sn-MFI as Lewis Acid Catalysts for Isomerization of Cellulosic Sugars. *ACS Catal.* **2014**, *4*, 2029–2037.
(27) Martens, J. A.; Verboekend, D.; Thomas, K.; Vanbutsele, G.; Pérez-Ramírez, J.; Gilson, J.-P. Hydroisomerization and Hydrocracking of Linear and Multibranched Long Model Alkanes on Hierarchical Pt/ZSM-22 Zeolite. *Catal. Today* **2013**, *218–219*, 135–142.
(28) Keller, T. C.; Isabettini, S.; Verboekend, D.; Rodrigues, E. G.; Perez-Ramirez, J. Hierarchical High-Silica Zeolites as Superior Base Catalysts. *Chem. Sci.* **2014**, *5*, 677–684.
(29) Zhang, H.; Hu, Z.; Huang, L.; Zhang, H.; Song, K.; Wang, L.; Shi, Z.; Ma, J.; Zhuang, Y.; Shen, W.; Zhang, Y.; Xu, H.; Tang, Y. Dehydration of Glycerol to Acrolein over Hierarchical ZSM-5 Zeolites: Effects of Mesoporosity and Acidity. *ACS Catal.* **2015**, *5*, 2548–2558.
(30) Chu, Y.; Yu, Z.; Zheng, A.; Fang, H.; Zhang, H.; Huang, S.-J.; Liu, S.-B.; Deng, F. Acidic Strengths of Brønsted and Lewis Acid Sites in Solid Acids Scaled by ^{31}P NMR Chemical Shifts of Adsorbed Trimethylphosphine. *J. Phys. Chem. C* **2011**, *115*, 7660–7667.
(31) Fang, H.; Zheng, A.; Li, S.; Xu, J.; Chen, L.; Deng, F. New Insights into the Effects of Acid Strength on the Solid Acid-Catalyzed Reaction: Theoretical Calculation Study of Olefinic Hydrocarbon Protonation Reaction. *J. Phys. Chem. C* **2010**, *114*, 10254–10264.
(32) Zheng, A.; Li, S.; Liu, S.-B.; Deng, F. Acidic Properties and Structure–Activity Correlations of Solid Acid Catalysts Revealed by Solid-State NMR Spectroscopy. *Acc. Chem. Res.* **2016**, *49*, 655–663.
(33) Wan, Z.; Wu, W.; Li, G.; Wang, C.; Yang, H.; Zhang, D. Effect of SiO_2/Al_2O_3 Ratio on the Performance of Nanocrystal ZSM-5

DOI: 10.1021/acs.iecr.8b00513
Ind. Eng. Chem. Res. 2018, 57, 8190–8199

Zeolite Catalysts in Methanol to Gasoline Conversion. *Appl. Catal., A* **2016**, *523*, 312−320.
(34) Ilias, S.; Khare, R.; Malek, A.; Bhan, A. A Descriptor for the Relative Propagation of the Aromatic- and Olefin-Based Cycles in Methanol-to-Hydrocarbons Conversion on H-ZSM-5. *J. Catal.* **2013**, *303*, 135−140.
(35) Svelle, S.; Joensen, F.; Nerlov, J.; Olsbye, U.; Lillerud, K.-P.; Kolboe, S.; Bjørgen, M. Conversion of Methanol into Hydrocarbons over Zeolite H-ZSM-5: Ethene Formation Is Mechanistically Separated from the Formation of Higher Alkenes. *J. Am. Chem. Soc.* **2006**, *128*, 14770−14771.
(36) Khare, R.; Liu, Z.; Han, Y.; Bhan, A. A Mechanistic Basis for the Effect of Aluminum Content on Ethene Selectivity in Methanol-to-Hydrocarbons Conversion on HZSM-5. *J. Catal.* **2017**, *348*, 300−305.
(37) Westgård Erichsen, M.; Svelle, S.; Olsbye, U. The Influence of Catalyst Acid Strength on the Methanol to Hydrocarbons (MTH) Reaction. *Catal. Today* **2013**, *215*, 216−223.
(38) Lee, K.-Y.; Lee, S.-W.; Ihm, S.-K. Acid Strength Control in MFI Zeolite for the Methanol-to-Hydrocarbons (MTH) Reaction. *Ind. Eng. Chem. Res.* **2014**, *53*, 10072−10079.
(39) Zhang, W.; Chu, Y.; Wei, Y.; Yi, X.; Xu, S.; Huang, J.; Zhang, M.; Zheng, A.; Deng, F.; Liu, Z. Influences of the Confinement Effect and Acid Strength of Zeolite on the Mechanisms of Methanol-to-Olefins Conversion over H-ZSM-5: A Theoretical Study of Alkenes-Based Cycle. *Microporous Mesoporous Mater.* **2016**, *231*, 216−229.
(40) Biligetu, T.; Wang, Y.; Nishitoba, T.; Otomo, R.; Park, S.; Mochizuki, H.; Kondo, J. N.; Tatsumi, T.; Yokoi, T. Al Distribution and Catalytic Performance of ZSM-5 Zeolites Synthesized with Various Alcohols. *J. Catal.* **2017**, *353*, 1−10.
(41) Liang, T.; Chen, J.; Qin, Z.; Li, J.; Wang, P.; Wang, S.; Wang, G.; Dong, M.; Fan, W.; Wang, J. Conversion of Methanol to Olefins over H-ZSM-5 Zeolite: Reaction Pathway Is Related to the Framework Aluminum Siting. *ACS Catal.* **2016**, *6*, 7311−7325.
(42) Sazama, P.; Wichterlová, B.; Tábor, E.; Šťastný, P.; Sathu, N. K.; Sobalík, Z.; Dědeček, J.; Sklenák, Š.; Klein, P.; Vondrová, A. Tailoring of the Structure of Fe-Cationic Species in Fe-ZSM-5 by Distribution of Al Atoms in the Framework for N_2O Decomposition and NH_3-SCR-NO_X. *J. Catal.* **2014**, *312*, 123−138.
(43) Wang, M.; Xia, Y.; Zhao, L.; Song, C.; Peng, L.; Guo, X.; Xue, N.; Ding, W. Remarkable Acceleration of the Fructose Dehydration over the Adjacent Brønsted Acid Sites Contained in an MFI-Type Zeolite Channel. *J. Catal.* **2014**, *319*, 150−154.
(44) Anderson, M. W.; Klinowski, J.; Xinsheng, L. Alumination of Highly Siliceous Zeolites. *J. Chem. Soc., Chem. Commun.* **1984**, 1596−1597.
(45) Chang, C. D.; Chu, C. T. W.; Miale, J. N.; Bridger, R. F.; Calvert, R. B. Aluminum Insertion into High Silica Zeolite Frameworks. 1. Reaction with Aluminum Halides. *J. Am. Chem. Soc.* **1984**, *106*, 8143−8146.
(46) Yamagishi, K.; Namba, S.; Yashima, T. Preparation and Acidic Properties of Aluminated ZSM-5 Zeolites. *J. Catal.* **1990**, *121*, 47−55.
(47) Dedecek, J.; Balgová, V.; Pashkova, V.; Klein, P.; Wichterlová, B. Synthesis of ZSM-5 Zeolites with Defined Distribution of Al Atoms in the Framework and Multinuclear MAS NMR Analysis of the Control of Al Distribution. *Chem. Mater.* **2012**, *24*, 3231−3239.
(48) Ma, D.; Deng, F.; Fu, R.; Han, X.; Bao, X. MAS NMR Studies on the Dealumination of Zeolite MCM-22. *J. Phys. Chem. B* **2001**, *105*, 1770−1779.
(49) Yang, G.; Wei, Y.; Xu, S.; Chen, J.; Li, J.; Liu, Z.; Yu, J.; Xu, R. Nanosize-Enhanced Lifetime of SAPO-34 Catalysts in Methanol-to-Olefin Reactions. *J. Phys. Chem. C* **2013**, *117*, 8214−8222.
(50) Wang, D.; Xu, S.; Yang, M.; Chu, Y.; Tian, P.; Liu, Z. Microporous Aluminophosphate ULM-6: Synthesis, NMR Assignment, and Its Transformation to $AlPO_4$-14 Molecular Sieve. *J. Phys. Chem. C* **2016**, *120*, 11854−11863.
(51) Lim, A. R.; Moon, H.-G.; Chang, J.-H. Nuclear Magnetic Resonance Study of the Phase Transitions and Local Environments of A-Alum $NH_4Al(SO_4)_2{\cdot}12H_2O$ Single Crystals. *Chem. Phys.* **2010**, *371*, 91−95.
(52) Barbera, K.; Bonino, F.; Bordiga, S.; Janssens, T. V. W.; Beato, P. Structure−Deactivation Relationship for ZSM-5 Catalysts Governed by Framework Defects. *J. Catal.* **2011**, *280*, 196−205.
(53) Fodor, D.; Beloqui Redondo, A.; Krumeich, F.; van Bokhoven, J. A. Role of Defects in Pore Formation in MFI Zeolites. *J. Phys. Chem. C* **2015**, *119*, 5447−5453.
(54) Li, J.; Liu, M.; Guo, X.; Xu, S.; Wei, Y.; Liu, Z.; Song, C. Interconnected Hierarchical ZSM-5 with Tunable Acidity Prepared by a Dealumination−Realumination Process: A Superior MTP Catalyst. *ACS Appl. Mater. Interfaces* **2017**, *9*, 26096−26106.
(55) Bleken, F. L.; Chavan, S.; Olsbye, U.; Boltz, M.; Ocampo, F.; Louis, B. Conversion of Methanol into Light Olefins over ZSM-5 Zeolite: Strategy to Enhance Propene Selectivity. *Appl. Catal., A* **2012**, *447−448*, 178−185.
(56) Mei, C.; Wen, P.; Liu, Z.; Liu, H.; Wang, Y.; Yang, W.; Xie, Z.; Hua, W.; Gao, Z. Selective Production of Propylene from Methanol: Mesoporosity Development in High Silica HZSM-5. *J. Catal.* **2008**, *258*, 243−249.
(57) Koempel, H.; Liebner, W. Lurgi's Methanol to Propylene (MTP) Report on a Successful Commercialisation. *Stud. Surf. Sci. Catal.* **2007**, *167*, 261−267.
(58) Deng, F.; Du, Y.; Ye, C.; Wang, J.; Ding, T.; Li, H. Acid Sites and Hydration Behavior of Dealuminated Zeolite HZSM-5: A High-Resolution Solid State NMR Study. *J. Phys. Chem.* **1995**, *99*, 15208−15214.
(59) Deng, F.; Yue, Y.; Ye, C. Observation of Nonframework Al Species in Zeolite B by Solid-State NMR Spectroscopy. *J. Phys. Chem. B* **1998**, *102*, 5252−5256.
(60) Gilson, J.-P.; Edwards, G. C.; Peters, A. W.; Rajagopalan, K.; Wormsbecher, R. F.; Roberie, T. G.; Shatlock, M. P. Penta-Co-Ordinated Aluminium in Zeolites and Aluminosilicates. *J. Chem. Soc., Chem. Commun.* **1987**, 91−92.
(61) Fischer, L.; Harlé, V.; Kasztelan, S.; d'Espinose de la Caillerie, J. B. Identification of Fluorine Sites at the Surface of Fluorinated γ-Alumina by Two-Dimensional MAS NMR. *Solid State Nucl. Magn. Reson.* **2000**, *16*, 85−91.
(62) Zheng, G.; Cui, X.; Huang, D.; Pang, J.; Mo, G.; Yu, S.; Tong, Z. Alkali-Activation Reactivity of Chemosynthetic Al_2O_3−SiO_2 Powders and Their ^{27}Al and ^{29}Si Magic-Angle Spinning Nuclear Magnetic Resonance Spectra. *Particuology* **2015**, *22*, 151−156.
(63) Burel, L.; Tuel, A. Nanozeolites: New Strategies for Designing Ultra Small Silicalite Crystals with Very Few Framework Defects. *Microporous Mesoporous Mater.* **2013**, *174*, 90−99.
(64) Khare, R.; Bhan, A. Mechanistic Studies of Methanol-to-Hydrocarbons Conversion on Diffusion-Free MFI Samples. *J. Catal.* **2015**, *329*, 218−228.
(65) Khare, R.; Millar, D.; Bhan, A. A Mechanistic Basis for the Effects of Crystallite Size on Light Olefin Selectivity in Methanol-to-Hydrocarbons Conversion on MFI. *J. Catal.* **2015**, *321*, 23−31.

DOI: 10.1021/acs.iecr.8b00513
Ind. Eng. Chem. Res. 2018, 57, 8190−8199